THE JOURNAL OF PHYSICAL CHEMISTRY Letters

Letter

pubs.acs.org/JPCL

Radiative Monomolecular Recombination Boosts Amplified Spontaneous Emission in $HC(NH_2)_2SnI_3$ Perovskite Films

Rebecca L. Milot, Giles E. Eperon, Thomas Green, Henry J. Snaith, Michael B. Johnston, and Laura M. Herz*

Department of Physics, University of Oxford, Clarendon Laboratory, Parks Road, Oxford OX1 3PU, United Kingdom

Supporting Information

ABSTRACT: Hybrid metal-halide perovskites have potential as cost-effective gain media for laser technology because of their superior optoelectronic properties. Although lead-halide perovskites have been most widely studied to date, tin-based perovskites have been proposed as a less toxic alternative. In this Letter, we show that amplified spontaneous emission (ASE) in formamidinium tin triiodide ($FASnI_3$) thin films is supported by an observed radiative monomolecular charge recombination pathway deriving from its unintentional doping. Such a radiative component will be active even at the lowest charge-carrier densities, opening a pathway for ultralow light-emission thresholds. Using time-resolved THz photoconductivity analysis, we further show that the material has an unprecedentedly high charge-carrier mobility of 22 $cm^2\ V^{-1}\ s^{-1}$ favoring efficient transport. In addition, $FASnI_3$ exhibits strong radiative bimolecular recombination and Auger rates that are over an order of magnitude lower than for lead-halide perovskites. In combination, these properties reveal that tin-halide perovskites are highly suited to light-emitting devices.

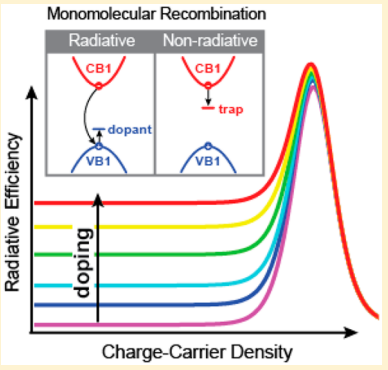

Hybrid metal halide perovskites are increasingly attracting attention as a class of low-cost semiconductors that can be easily synthesized via solution processing or vapor deposition techniques.[1,2] Their favorable optoelectronic properties include high charge-carrier mobility, long charge-carrier lifetimes, high absorption coefficients, long charge-carrier diffusion lengths, and synthetic tunability.[3,4] The recent focus has mostly been on photovoltaics, and perovskite-based cells now boast power conversion efficiencies in excess of 22%, rivaling existing silicon technologies.[5] However, a good photovoltaic material should also lend itself effectively to the reverse process—light emission. Hence, promising reports of LEDs and lasing are emerging.[6−8] Lasing is a particularly suitable application since there is currently a high demand for cost-effective laser diodes that can be assembled on chips using simple synthetic means. That said, many of the existing solution-processed materials have struggled to be competitive with traditional inorganic semiconductors currently implemented in laser diodes.[7] For example, organic semiconductors are limited by low charge-carrier mobility, low damage threshold, and losses due to exciton−exciton annihilation,[7,9,10] whereas colloidal quantum dots suffer from high Auger recombination rates that compete with photoemission.[7] Hybrid metal halide perovskites, on the other hand, offer a promising alternative because of their low defect densities, high charge-carrier mobilities, and high photoluminescence (PL) quantum yield.[7] Amplified spontaneous emission (ASE) and lasing have been reported for a range of hybrid perovskite materials including thin films, nanowires, and nanoparticles.[6,7,11−17] Reported ASE thresholds vary from less than 10 $\mu J/cm^2$ to over 100 $\mu J/cm^2$, which are values already competitive with those of leading solution processed materials including organic semiconductors and quantum dots.[6,7,9,18] Hybrid perovskite lasing through optical pumping has been demonstrated with a variety of cavity configurations, exhibiting high gain and Q-factors up to 3600.[6,7] Furthermore, tunable lasing has been demonstrated at wavelengths ranging from the visible to the near-infrared,[6,13] opening up a wide range of potential applications including spectroscopy, imaging, data storage, and telecommunications.

Most of the studies of ASE and lasing in hybrid metal-halide perovskites have focused on lead-based perovskites such as methylammonium lead triiodide ($MAPbI_3$) and cesium lead triiodide.[6,7] However, toxicity is a main deterrent for using lead perovskites for optoelectronic applications.[19,20] For example, the European Union's RoHS compliance guidelines on electrical and electronic equipment limit lead content to less than 1000 ppm (there is an exemption for renewable energy technologies such as photovoltaic cells but not for lasers).[21] Varying legislation across different countries could make worldwide commercialization of light-emitting devices with lead-based materials difficult. Tin-based perovskites have therefore been proposed as a less toxic alternative.[13,22−24] Initial photovoltaic studies with hybrid tin perovskites have yielded power conversion efficiencies (PCEs) limited to below 6%, which is much lower than the record of now over 22% for

Received: September 6, 2016
Accepted: October 5, 2016
Published: October 7, 2016

DOI: 10.1021/acs.jpclett.6b02030
J. Phys. Chem. Lett. 2016, 7, 4178−4184

lead-based systems.[5,22,24,25] This decreased efficiency has been attributed to p-doping, occurring as a result of a low formation energy of tin vacancies.[26−28] The additional holes released from dopant sites contribute to an enhanced monomolecular charge-carrier recombination rate, which decreases the diffusion length and leads to less efficient charge transport in the thin film.[5,22,24,25] Accordingly, decreasing the doping concentration by adding excess Sn^{2+} to the precursor solution has resulted in improved PCEs.[23,29] Although such p-doping is clearly detrimental for photovoltaics, it can be advantageous for lasing applications, given that the additional monomolecular recombination pathway between electrons and holes released from dopants should be radiative for a direct band gap semiconductor. An enhanced radiative recombination pathway in the low charge-density regime would be highly beneficial for lasing because the ASE threshold is determined by the radiative lifetime and the overall lasing efficiency is governed by the radiative efficiency of the material.[30] For example, a recent report on GaAs nanowire lasers has demonstrated that it is possible to exploit p-doping specifically to improve radiative efficiency and decrease the ASE threshold.[31] Here, we conclusively show that formamidinium tin triiodide ($FASnI_3$) also displays such highly desirable monomolecular radiative charge-carrier decay channels. We demonstrate that thin films of $FASnI_3$ exhibit ASE at moderate threshold charge-carrier densities and analyze the recombination dynamics above and below threshold. We find that $FASnI_3$ exhibits an advantageous combination of a radiative bimolecular recombination rate constant similar to GaAs and an Auger rate constant much lower than those reported for lead-based perovskites. In combination with a high charge-carrier mobility, this lead-free material therefore displays highly favorable properties for light emission and lasing.

$FASnI_3$ thin films were synthesized via spin-coating onto z-cut quartz substrates using a solvent quenching approach, which enables the production of high quality, smooth, and continuous films (details in the Methods section). The resulting films were 380 nm thick and highly crystalline as we show in Figure S1A of the Supporting Information (SI). UV−visible absorption measurements revealed a band edge centered near 860 nm (1.44 eV) and high absorption coefficients approaching 1×10^5 cm^{-1} at shorter wavelengths (see Figure S1B of the SI). We determine a charge-carrier mobility of 22 cm^2 V^{-1} s^{-1} for the $FASnI_3$ thin films using contact-free optical pump−THz probe (OPTP) spectroscopy (see the SI for details on the charge-carrier mobility calculation).[32] This value is an order of magnitude higher than initial reports for tin perovskite thin films[22,23] and more comparable to the best performing lead-based films,[3] suggesting that lasing in these $FASnI_3$ thin films should not be limited by low charge-carrier mobility as it has been in organic semiconductors.[9] Furthermore, high charge-carrier mobility is essential for electrically pumped lasing, which eliminates the need for optical pumping and thus facilitates miniaturization and chip integration.[5,33]

We demonstrate ASE in $FASnI_3$ thin films by evaluating the changes in the photoluminescence (PL) spectrum following photoexcitation at 800 nm with increasing excitation fluence and corresponding photogenerated charge-carrier densities (Figure 1A,B). In the low-density regime (<6×10^{17} cm^{-3}) the PL peak is centered at 896 nm (1.38 eV), which corresponds to a Stokes shift from the absorption spectrum of 60 meV. This value is low compared to $MASnI_3$ (200 meV)[26] and nearer that for $MAPbI_3$ (10 meV),[34] suggesting

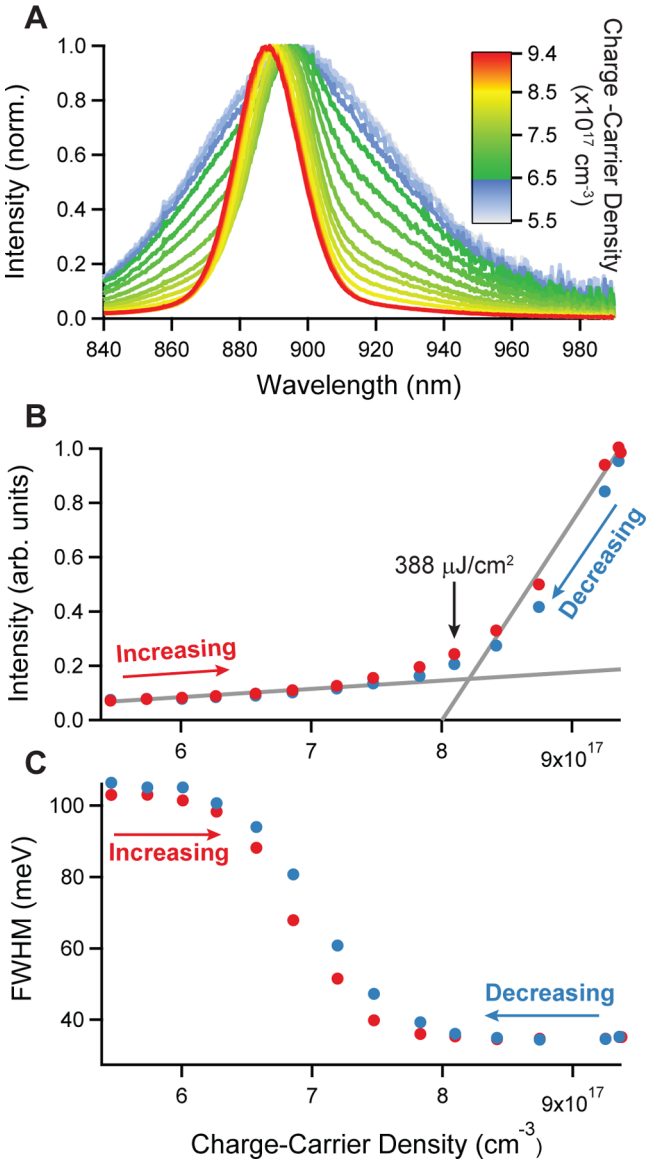

Figure 1. (A) PL spectra obtained following photoexcitation at 800 nm. Spectra were acquired while increasing the fluence such that the carrier densities ranged from 5.5×10^{17} cm^{-3} to 9.4×10^{17} cm^{-3}. Laser excitation fluences were converted to charge-carrier density, taking into account the nonlinear relationship at high fluence between the incident fluence and the resulting charge-carrier density in the film (Figure S2). Additionally, reported charge-carrier densities have been averaged to account for the finite charge-carrier lifetime and sample thickness (see SI for further details). Spectra obtained while decreasing the carrier density are included in Figure S3. (B) Integrated PL intensity as a function of average charge-carrier density. Values were obtained as the excitation intensity was first increased (red dots) and then decreased (blue dots). The solid gray lines indicate an ASE threshold at an average charge-carrier density of approximately 8×10^{17} cm^{-3}. (C) Changes in FWHM of the PL peak with increasing (red dots) and decreasing (blue dots) carrier density.

that the substitution of FA for MA and the improved processing techniques used here significantly lower energetic disorder. This observation is consistent with the improved charge-carrier mobility we find for $FASnI_3$, which is more than an order of magnitude higher than values reported for $MASnI_3$ thin films.[5,22,24,25] A low Stokes shift is important for lasing applications because it prevents additional energy losses that

DOI: 10.1021/acs.jpclett.6b02030
J. Phys. Chem. Lett. 2016, 7, 4178−4184

are dissipated as heat.[7] In addition to the decreased Stokes shift, the full-width-at-half-maximum (FWHM) of 110 meV (Figure 1C) is lower than previously reported for $MASnI_3$.[26] This decrease is most likely also the result of improved materials properties of these $FASnI_3$ films, although changes in electron−phonon coupling may also play a role.[35] As the excitation fluence is increased, the FWHM begins to decrease until reaching 35 meV at 8×10^{17} cm^{-3}, indicating that ASE is occurring. At carrier densities above 8×10^{17} cm^{-3}, the intensity begins to deviate from its linear trend, which is an additional marker for ASE. Taken together, the two intensity trends mark an ASE threshold of approximately 8×10^{17} cm^{-3}, which is within the range of values reported for other perovskite materials and comparable to other thin film technologies.[5,6,9,18] At high carrier densities, the PL peak maximum gradually blue shifts until reaching 889 nm (1.4 eV) at a carrier density of 9.4×10^{17} cm^{-3}. This shift is most likely the result of lattice heating because the band gaps of both tin and lead perovskites are known to blue shift with increasing temperature.[26,34] Nearly identical results were obtained with first increasing and then decreasing excitation fluence, indicating that none of the observed changes were a result of damaging the sample.

We proceed by analyzing the charge-carrier dynamics in $FASnI_3$ both below and at the ASE threshold using OPTP spectroscopy (Figure 2). In OPTP spectroscopy, the change in the broadband THz absorption is monitored as a function of the time delay between an optical pump pulse and THz probe pulse. Because mobile electrons decrease the transmission at THz frequencies, changes in the THz intensity ($\Delta T/T$) can be attributed to changes in conductivity. As a result, $\Delta T/T$ is proportional to the photoconductivity and thus to the charge-carrier mobility multiplied with the charge-carrier density.[36−38] Therefore, the decay in signal toward positive time delay can be attributed to charge-carrier recombination assuming that the charge-carrier mobility is constant.

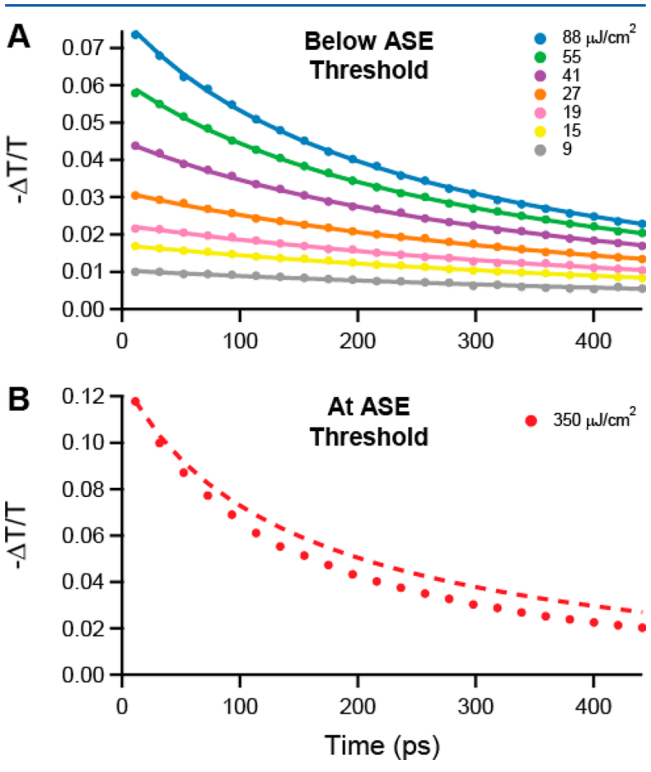

Figure 2. (A) Charge-carrier dynamics in $FASnI_3$ below the ASE threshold. The film was photoexcited at 800 nm with fluences ranging from 9−88 $\mu J/cm^2$. The dots indicate experimental data, and the solid lines are fits to eq 1. (B) Charge-carrier dynamics at the ASE threshold. The film was photoexcited at 800 nm with a fluence of 350 $\mu J/cm^2$. The red dots represent experimental data, and the dashed red line is calculated from the fitting parameters obtained in part A and represents the predicted carrier dynamics at this fluence assuming an absence of ASE.

An understanding of the overall charge-carrier recombination dynamics is important because efficient lasing requires the preference of radiative recombination over the various nonradiative processes that can occur. Though OPTP measurements by themselves will not reveal which of these mechanisms are radiative, further examination of the underlying processes may help. For example, because these lead and tin-based perovskites are predominantly direct band gap semiconductors, the bimolecular band-to-band recombination between electrons and holes should be radiative.[4] Auger recombination on the other hand, which involves electron−hole recombination through energy transfer to a third charge-carrier, is nonradiative and is a significant concern for lasing because it directly competes with bimolecular recombination at the high charge-carrier densities required for lasing.[3,4] High Auger rates are one of the major limits to quantum dots and many other thin film technologies,[18,39] and significant synthetic effort has been dedicated to decreasing these values. Finally, monomolecular recombination can be either radiative or nonradiative depending on the mechanism involved.[31] Hence following photoexcitation, the dynamic charge-carrier recombination processes in a p-doped material can be described by the following rate equation:

$$\begin{aligned} \frac{dn}{dt} &= -k_3 n^3 - k_2 n(p + p_0) - k_1^{nr} n \\ &= -k_3 n^3 - k_2 n^2 - k_1^{total} n \\ &= -R_T n \end{aligned} \quad (1)$$

where k_2 is the bimolecular recombination rate constant, k_3 is the third-order or Auger recombination rate constant, and $R_T = k_3 n^2 + k_2 n + k_1^{total}$ is the effective total recombination rate. Here, we reasonably assume that the density of photogenerated electrons equals the density of photogenerated holes ($n = p$). The monomolecular recombination rate $k_1^{total} = k_2 p_0 + k_1^{nr}$ thus comprises two contributions: the first term ($k_1^r = k_2 p_0$) is mediated by the recombination of photogenerated electrons (n) with a constant dopant hole density (p_0) which should be radiative as it is fundamentally the same mechanism as the bimolecular recombination of photogenerated electrons (n) with photogenerated holes ($p = n$). The presence of doping hence introduces a radiative "pseudo-monomolecular" decay component at low charge-carrier densities. The second term (k_1^{nr}) is caused by Shockley−Read−Hall (SRH) recombination,[40] which is mediated by traps that may act as recombination centers if both types of carriers are caught. In this case, charge-recombination tends to be nonradiative. Such Shockley−Read−Hall recombination appears to be the dominant process at low charge density for lead-based halide perovskites that exhibit nonradiative monomolecular rates attributed to charge-carrier capture into traps.[4,41,42] In contrast, tin-based perovskites may potentially exhibit radiative mono-

DOI: 10.1021/acs.jpclett.6b02030
J. Phys. Chem. Lett. 2016, 7, 4178−4184

molecular decay channels because of their unintentionally high levels of p-doping as discussed above.

To analyze the recombination parameters for these processes, the recombination dynamics in $FASnI_3$ were fitted to eq 1 for excitation fluences below the ASE threshold (Figure 2A). A global fit across all of the fluences yields $k_1 = 1.2 \times 10^9$ s^{-1}, $k_2 = 2.3 \times 10^{-10}$ cm^3 s^{-1}, and $k_3 = 9.3 \times 10^{-30}$ cm^6 s^{-1}. The first notable observation is that the Auger recombination rate constant (k_3) is over an order of magnitude lower than that typically found for lead-based hybrid perovskites[3] and is similar to that for GaAs.[43] Such low Auger rates suggest that tin-based perovskites can exhibit much higher radiative efficiencies at high charge-carrier densities than colloidal quantum dots and lead-based perovskites.[6,7] We propose that the lower Auger rates for tin compared with lead iodide perovskites may be the direct result of the lower spin−orbit coupling (SOC) in the perovskites incorporating the lighter tin atoms.[44,45] Such changes in SOC can profoundly affect the energy levels of spin-split-off states in the conduction band, which may be involved in the Auger recombination process. In particular, DFT calculations including SOC show that the splitting between the lowest conduction bands in lead perovskites such as $CsPbI_3$ is similar to its band gap energy.[46] This scenario may allow efficient near-vertical Auger transitions that satisfy the need for energy and momentum conservation, as is the case in GaSb.[47] For tin perovskites such as $CsSnI_3$, on the other hand, the conduction band splitting is much smaller than the band gap energy,[44] which may reduce such Auger mechanisms substantially. Our observations suggest that tin halide perovskites therefore are intrinsically much more suitable than lead halide perovskites for applications requiring high charge carrier densities. Examining the value of the bimolecular charge recombination constant (k_2) extracted for $FASnI_3$, we find this to be comparable to that of GaAs and the best lead-based perovskites measured, suggesting strong radiative band-to-band recombination. The monomolecular recombination rate we observe for $FASnI_3$ is significantly lower than previously reported for $MASnI_3$,[22] consistent with the improvement of film quality as discussed previously. However, through the more subtle analysis presented below, we will demonstrate that monomolecular recombination is partially radiative and that a high k_1 value is not necessarily detrimental to lasing for $FASnI_3$.

In addition, we analyze the charge-carrier recombination dynamics occurring at the ASE threshold, where we find charge-carrier recombination to accelerate. As seen in Figure 2B, the decay is faster in the presence of ASE (red dots) than it would be assuming that ASE is not occurring (dashed, black line, based on charge-recombination constants extracted for data below ASE threshold). We attribute this increased recombination rate to a relative increase in radiative recombination, as it concurs with the observed rapid increase in emission intensity at the threshold. This effect is hence another indicator of amplified emission in which the presence of the photon density inside the film enhances radiative emission.[13,48]

Although an analysis of OPTP data alone may not reveal the radiative nature of a recombination mechanism, its combination with radiative efficiency data can provide very conclusive results.[3,4] To further analyze the mechanisms of monomolecular recombination, we carefully determined the relative radiative efficiency over the low charge-carrier density regime spanning more than 6 decades of excitation fluences below the ASE threshold (Figure 3). In general, the radiative efficiency

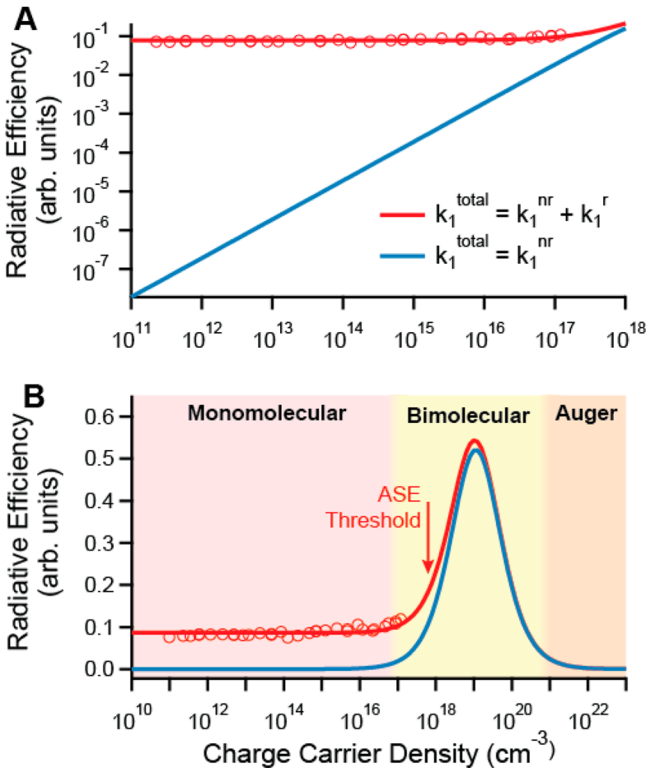

Figure 3. Radiative efficiency as a function of average carrier density. For the experimental data (open, red circles), the $FASnI_3$ film was photoexcited at 790 nm with fluences ranging from 1.1 pJ/cm^2 to 2.1 $\mu J/cm^2$. The solid red line is a fit to eq 2, and the solid blue line was calculated using eq 2 and setting $k_1^r = 0$. Part A highlights the experimentally accessible range of carrier densities, and part B includes a wider range of carrier densities to highlight the monomolecular, bimolecular, and Auger−dominated regimes.

(the number of photons emitted per photons absorbed) is given by the ratio of radiative charge-carrier recombination rates over that of all (radiative and nonradiative) rates.[3,4] Following our above arguments of purely radiative bimolecular recombination, and purely nonradiative Auger recombination, the radiative efficiency $\Phi(n)$ in the absence of ASE then depends on the charge-carrier density through

$$\Phi(n) = \frac{k_1^r + nk_2}{k_1^{total} + nk_2 + n^2k_3} \quad (2)$$

where k_1^r is the radiative (dopant mediated) component of the monomolecular recombination, k_1^{nr} is the nonradiative (SRH) component, and $k_1^{total} = k_1^r + k_1^{nr}$. We note that because the values of k_1^{total}, k_2, and k_3 are already determined from OPTP measurements, fits of eq 2 to the radiative efficiency data displayed in Figure 3 will allow for a highly accurate separation of k_1^{total} into its radiative and nonradiative parts. However, a qualitative assessment of whether radiative recombination contributes to the monomolecular decay in $FASnI_3$ can already be made from the functional form of the data in the low charge-carrier density regime. For the case of purely nonradiative monomolecular decay ($k_1^r = 0$), eq 2 approximates to $\Phi(n) \sim nk_2/k_1^{total}$, that is, the function should linearly approach the origin as shown by the blue line in Figure 3A. However, comparison with the data shows that this is clearly not the case; rather, the data approach a constant value toward low charge-carrier density. This is exactly as would be expected in the

DOI: 10.1021/acs.jpclett.6b02030
J. Phys. Chem. Lett. 2016, 7, 4178−4184

presence of a radiative contribution to k_1^{total}, for which eq 2 approaches $\Phi(n) \sim k_1^r/k_1^{total}$ at low charge-carrier densities. The functional form of the radiative efficiency data therefore clearly demonstrates that monomolecular recombination in $FASnI_3$ has radiative contributions.

To quantify this contribution, eq 2 was fit to the experimental data with the values of k_1^{total}, k_2, and k_3 determined from OPTP measurements (Figure 3). With the inclusion of a scaling parameter, the fit yielded a value of $k_1^r = 1.1 \times 10^8$ s^{-1}, indicating that about one tenth of the monomolecular recombination in this material is radiative. Because this radiative contribution most likely originates from unintentional hole doping, the hole-doping density p_0 can be calculated using $k_1^r = p_0 k_2$ to be 4.8×10^{17} cm^{-3}, which is similar to doping densities estimated from Hall measurements on $MASnI_3$ single crystals.[22,49] In general, doping levels will depend on the exact processing and treatments used for tin perovskites and will therefore be a tunable parameter.[13,23,29] The unintentional doping level we report for $FASnI_3$ here is at least 2 orders of magnitude above typical estimates for hybrid lead halide perovskites,[50−52] which explains why radiative contributions to the monomolecular decay channels are not typically observed in past studies of lead-based perovskites.[41,42] However, recent studies of methylammonium lead iodide perovskite films have shown that passivation with Lewis bases can lead to PL lifetimes in the microsecond regime, for which radiative monomolecular components may then also begin to emerge.[53] The relative presence of such radiative contributions in the low charge-density regime hence is influenced by the relative trade-off between dopant concentration and trap-mediated (SHR) recombination.

Figure 3B extends the radiative efficiency curves (eq 2) to higher charge carrier densities. The red curve shows the actual values in the presence of a radiative monomolecular component, whereas the blue curve shows the expected behavior for purely nonradiative (SRH) monomolecular decay. The peak near $n \sim 10^{19}$ cm^{-3} indicates the range of charge-carrier densities where bimolecular radiative recombination dominates. Not surprisingly, the measured threshold for ASE near 8×10^{17} cm^{-3} corresponds to the onset of strong bimolecular recombination. Hence the radiative efficiency is still limited at the high end by Auger recombination and on the low end by monomolecular recombination. However, the radiative component of the monomolecular recombination distinctly raises the radiative efficiency at low charge-carrier densities and also at the peak; hence, it must contribute to lower the ASE threshold and therefore ultimately yield more efficient lasing.[30,31] In addition, the ASE threshold could be lowered further through a reduction of the nonradiative component of the monomolecular decay channels that may originate from traps caused by a variety of vacancies, interstitials, or substitutions[28] because this would increase the relative radiative contribution in the low charge-density regime. Therefore, the unintentional p-doping encountered in tin halide perovskites can open the door for lasing thresholds that are substantially reduced[13,22−24] with respect to the current lead-based perovskites. We also note that the concept of doping is already used extensively in the well-established field of inorganic semiconductor light-emitting diodes, where deliberate introduction of dopant gradients allows control over light-emission at p−n junctions[54] and enhances radiative recombination.[31] Attaining better control over p-doping in tin based perovskites and implementing combinations with suitable n-doped materials can therefore open interesting possibilities for highly efficient hybrid perovskite light-emitting diodes.

In conclusion, we have demonstrated and analyzed ASE in $FASnI_3$ thin films exhibiting a threshold charge-carrier density of 8×10^{17} cm^{-3}. We find that $FASnI_3$ is highly suited to lasing applications because it exhibits high charge-carrier mobility in combination with very low Auger and strong radiative bimolecular recombination rate constants similar to GaAs. We further show that, unlike typical lead-based halide perovskites, $FASnI_3$ displays a radiative monomolecular recombination pathway, which we attribute to its unintentional p-doping with relatively high doping density near 5×10^{17} cm^{-3}. Such a radiative component will be active even at the lowest charge-carrier densities, opening a pathway for ultralow ASE thresholds. All of these properties indicate that $FASnI_3$ is a promising lead-free material for realizing low-cost, on-chip laser diodes, which are in high demand for many optoelectronic applications.[7]

EXPERIMENTAL METHODS

Synthesis of $FASnI_3$ Thin Films. $FASnI_3$ thin films were prepared from a mixture of a 1:1 molar ratio of FAI to SnI_2 at 1 M in a mixed solvent of DMF:DMSO 65:35 by volume. Excess 0.2 M SnF_2 was added into the precursor solution (i.e., providing a 20% excess of Sn^{2+}). The precursor solution was spin-coated onto oxygen plasma-cleaned z-cut quartz substrates dynamically at 7000 rpm for 1 s in a nitrogen-filled glovebox and subsequently immersed into a Petri dish containing an antisolvent (anisole) for 5s. The film was dried with a nitrogen gun and annealed at 70 °C for 20 min.

Steady-State PL Spectra. To obtain steady-state PL spectra, the films were photoexcited at 800 nm using an amplified laser system (Spectra Physics, Millennia-Tsunami-Empower-Spitfire) with a 40 fs pulse width and 1.1 kHz repetition rate. PL spectra were collected at fluences ranging from 159−795 $\mu J/cm^2$ using a UV−vis mini spectrometer (Ocean Optics, USB2000+) fitted with an optical fiber, a collimating lens, and an 850 nm long-pass filter.

Optical-Pump THz Probe (OPTP) Spectroscopy. The OPTP setup uses the output of an amplified laser (Millennia-Tsunami-Empower-Spitfire), which is centered at 800 nm, has a repetition rate of 1 kHz, and has a pulse duration of 40 fs. Portions of the laser beam were used to generate THz radiation via optical rectification in a 450-μm thick GaP(110) crystal and to detect it via free-space electro-optic sampling in a ZnTe crystal (0.2 mm ZnTe(110) on 3 mm ZnTe(100)). The remainder of the beam was used to photoexcite the sample. Charge-carrier recombination dynamics are obtained by monitoring the change in peak THz amplitude ($\Delta T/T$) as a function of the delay between the optical pump pulse and the THz probe pulse. All of the measurements were performed with the entire THz beam path and sample in vacuum.

Radiative Efficiency. The thin films were photoexcited with a Ti:sapphire oscillator (Mai Tai, Spectra Physics), which has a pulse duration of 80 fs and a repetition rate of 80 MHz. The center wavelength was tuned to 790 nm. Photoluminescence from the sample was collected by a pair of off-axis parabolic mirrors, focused onto a grating monochromator (Triax, Horiba), and detected using a nitrogen-cooled Si-CCD detector (Symphony, Horiba).

DOI: 10.1021/acs.jpclett.6b02030
J. Phys. Chem. Lett. 2016, 7, 4178−4184

■ ASSOCIATED CONTENT

Supporting Information

The Supporting Information is available free of charge on the ACS Publications website at DOI: 10.1021/acs.jpclett.6b02030.

Film characterization, determination of average carrier density, additional PL spectra, charge-carrier mobility calculation, and fits to THz photoconductivity transients. (PDF)

■ AUTHOR INFORMATION

Corresponding Author

*E-mail: laura.herz@physics.ox.ac.uk.

Present Address

(G.E.E.) Department of Chemistry, University of Washington, Seattle, Washington 98105, United States.

Notes

The authors declare no competing financial interest.

■ ACKNOWLEDGMENTS

The authors thank the Engineering Physical Sciences Research Council (EPSRC) for financial support.

■ REFERENCES

(1) Jung, H. S.; Park, N. G. Perovskite Solar Cells: From Materials to Devices. *Small* **2015**, *11*, 10−25.

(2) Liu, M. Z.; Johnston, M. B.; Snaith, H. J. Efficient Planar Heterojunction Perovskite Solar Cells by Vapour Deposition. *Nature* **2013**, *501*, 395−398.

(3) Johnston, M. B.; Herz, L. M. Hybrid Perovskites for Photovoltaics: Charge-Carrier Recombination, Diffusion, and Radiative Efficiencies. *Acc. Chem. Res.* **2016**, *49*, 146−154.

(4) Herz, L. M. Charge-Carrier Dynamics in Organic-Inorganic Metal Halide Perovskites. *Annu. Rev. Phys. Chem.* **2016**, *67*, 65−89.

(5) Manser, J. S.; Christians, J. A.; Kamat, P. V. Intriguing Optoelectronic Properties of Metal Halide Perovskites. *Chem. Rev.* **2016**, DOI: 10.1021/acs.chemrev.6b00136.

(6) Veldhuis, S. A.; Boix, P. P.; Yantara, N.; Li, M.; Sum, T. C.; Mathews, N.; Mhaisalkar, S. G. Perovskite Materials for Light-Emitting Diodes and Lasers. *Adv. Mater.* **2016**, *28*, 6804.

(7) Sutherland, B. R.; Sargent, E. H. Perovskite Photonic Sources. *Nat. Photonics* **2016**, *10*, 295−302.

(8) Fang, Y. J.; Dong, Q. F.; Shao, Y. C.; Yuan, Y. B.; Huang, J. S. Highly Narrowband Perovskite Single-Crystal Photodetectors Enabled by Surface-Charge Recombination. *Nat. Photonics* **2015**, *9*, 679−686.

(9) Grivas, C.; Pollnau, M. Organic Solid-State Integrated Amplifiers and Lasers. *Laser Photon. Rev.* **2012**, *6*, 419−462.

(10) Samuel, I. D. W.; Turnbull, G. A. Organic Semiconductor Lasers. *Chem. Rev.* **2007**, *107*, 1272−1295.

(11) Deschler, F.; Price, M.; Pathak, S.; Klintberg, L. E.; Jarausch, D. D.; Higler, R.; Huttner, S.; Leijtens, T.; Stranks, S. D.; Snaith, H. J.; et al. High Photoluminescence Efficiency and Optically Pumped Lasing in Solution-Processed Mixed Halide Perovskite Semiconductors. *J. Phys. Chem. Lett.* **2014**, *5*, 1421−1426.

(12) Saliba, M.; Wood, S. M.; Patel, J. B.; Nayak, P. K.; Huang, J.; Alexander-Webber, J. A.; Wenger, B.; Stranks, S. D.; Horantner, M. T.; Wang, J. T. W.; et al. Structured Organic-Inorganic Perovskite toward a Distributed Feedback Laser. *Adv. Mater.* **2016**, *28*, 923−929.

(13) Xing, G.; Kumar, M. H.; Chong, W. K.; Liu, X.; Cai, Y.; Ding, H.; Asta, M.; Grätzel, M.; Mhaisalkar, S.; Mathews, N.; et al. Solution-Processed Tin-Based Perovskite for Near-Infrared Lasing. *Adv. Mater.* **2016**, DOI: 10.1002/adma.201601418.

(14) Xing, G. C.; Mathews, N.; Lim, S. S.; Yantara, N.; Liu, X. F.; Sabba, D.; Gratzel, M.; Mhaisalkar, S.; Sum, T. C. Low-Temperature Solution-Processed Wavelength-Tunable Perovskites for Lasing. *Nat. Mater.* **2014**, *13*, 476−480.

(15) Yakunin, S.; Protesescu, L.; Krieg, F.; Bodnarchuk, M. I.; Nedelcu, G.; Humer, M.; De Luca, G.; Fiebig, M.; Heiss, W.; Kovalenko, M. V. Low-Threshold Amplified Spontaneous Emission and Lasing from Colloidal Nanocrystals of Caesium Lead Halide Perovskites. *Nat. Commun.* **2015**, *6*, 8056.

(16) Zhu, H. M.; Fu, Y. P.; Meng, F.; Wu, X. X.; Gong, Z. Z.; Ding, Q.; Gustafsson, M. V.; Trinh, M. T.; Jin, S.; Zhu, X. Y. Lead Halide Perovskite Nanowire Lasers with Low Lasing Thresholds and High Quality Factors. *Nat. Mater.* **2015**, *14*, 636−642.

(17) Stranks, S. D.; Wood, S. M.; Wojciechowski, K.; Deschler, F.; Saliba, M.; Khandelwal, H.; Patel, J. B.; Elston, S. J.; Herz, L. M.; Johnston, M. B.; et al. Enhanced Amplified Spontaneous Emission in Perovskites Using a Flexible Cholesteric Liquid Crystal Reflector. *Nano Lett.* **2015**, *15*, 4935−4941.

(18) Klimov, V. I. Multicarrier Interactions in Semiconductor Nanocrystals in Relation to the Phenomena of Auger Recombination and Carrier Multiplication. In *Annual Reviews of Condensed Matter Physics*; Langer, J. S., Ed.; Annual Reviews: Palo Alto, CA, **2014**; Vol. 5, pp 285−31610.1146/annurev-conmatphys-031113-133900.

(19) Benmessaoud, I. R.; Mahul-Mellier, A. L.; Horvath, E.; Maco, B.; Spina, M.; Lashuel, H. A.; Forro, L. Health Hazards of Methylammonium Lead Iodide Based Perovskites: Cytotoxicity Studies. *Toxicol. Res.* **2016**, *5*, 407−419.

(20) Zhang, J. Y.; Gao, X. F.; Deng, Y. L.; Li, B. B.; Yuan, C. Life Cycle Assessment of Titania Perovskite Solar Cell Technology for Sustainable Design and Manufacturing. *ChemSusChem* **2015**, *8*, 3882−3891.

(21) *Directive 2011/65/EU of the European Parliament and of the Council of 8 June 2011 on the Restriction of the Use of Certain Hazardous Substances in Electrical and Electronic Equipment*; Official Journal of the European Union: European Union, 2011.

(22) Noel, N. K.; Stranks, S. D.; Abate, A.; Wehrenfennig, C.; Guarnera, S.; Haghighirad, A. A.; Sadhanala, A.; Eperon, G. E.; Pathak, S. K.; Johnston, M. B.; et al. Lead-Free Organic-Inorganic Tin Halide Perovskites for Photovoltaic Applications. *Energy Environ. Sci.* **2014**, *7*, 3061−3068.

(23) Kumar, M. H.; Dharani, S.; Leong, W. L.; Boix, P. P.; Prabhakar, R. R.; Baikie, T.; Shi, C.; Ding, H.; Ramesh, R.; Asta, M.; et al. Lead-Free Halide Perovskite Solar Cells with High Photocurrents Realized Through Vacancy Modulation. *Adv. Mater.* **2014**, *26*, 7122−7127.

(24) Hao, F.; Stoumpos, C. C.; Cao, D. H.; Chang, R. P. H.; Kanatzidis, M. G. Lead-Free Solid-State Organic-Inorganic Halide Perovskite Solar Cells. *Nat. Photonics* **2014**, *8*, 489−494.

(25) Koh, T. M.; Krishnamoorthy, T.; Yantara, N.; Shi, C.; Leong, W. L.; Boix, P. P.; Grimsdale, A. C.; Mhaisalkar, S. G.; Mathews, N. Formamidinium Tin-Based Perovskite with Low E-g for Photovoltaic Applications. *J. Mater. Chem. A* **2015**, *3*, 14996−15000.

(26) Parrott, E. S.; Milot, R. L.; Stergiopoulos, T.; Snaith, H. J.; Johnston, M. B.; Herz, L. M. Effect of Structural Phase Transition on Charge-carrier Lifetimes and Defects in $CH_3NH_3SnI_3$ Perovskite. *J. Phys. Chem. Lett.* **2016**, *7*, 1321−1326.

(27) Chung, I.; Song, J. H.; Im, J.; Androulakis, J.; Malliakas, C. D.; Li, H.; Freeman, A. J.; Kenney, J. T.; Kanatzidis, M. G. CsSnI3: Semiconductor or Metal? High Electrical Conductivity and Strong Near-Infrared Photoluminescence from a Single Material. High Hole Mobility and Phase-Transitions. *J. Am. Chem. Soc.* **2012**, *134*, 8579−8587.

(28) Xu, P.; Chen, S. Y.; Xiang, H. J.; Gong, X. G.; Wei, S. H. Influence of Defects and Synthesis Conditions on the Photovoltaic Performance of Perovskite Semiconductor $CsSnI_3$. *Chem. Mater.* **2014**, *26*, 6068−6072.

(29) Marshall, K. P.; Walton, R. I.; Hatton, R. A. Tin Perovskite/Fullerene Planar Layer Photovoltaics: Improving the Efficiency and Stability of Lead-Free Devices. *J. Mater. Chem. A* **2015**, *3*, 11631−11640.

(30) Peters, G. I.; Allen, L. Amplified Spontaneous Emission. 1. Threshold Condition. *J. Phys. A: Gen. Phys.* **1971**, *4*, 238−243.

(31) Burgess, T.; Saxena, D.; Mokkapati, S.; Li, Z.; Hall, C. R.; Davis, J. A.; Wang, Y.; Smith, L. M.; Fu, L.; Caroff, P.; et al. Doping-

DOI: 10.1021/acs.jpclett.6b02030
J. Phys. Chem. Lett. 2016, 7, 4178−4184

Enhanced Radiative Efficiency Enables Lasing in Unpassivated GaAs Nanowires. *Nat. Commun.* **2016**, *7*, 11927.
(32) Wehrenfennig, C.; Eperon, G. E.; Johnston, M. B.; Snaith, H. J.; Herz, L. M. High Charge Carrier Mobilities and Lifetimes in Organolead Trihalide Perovskites. *Adv. Mater.* **2014**, *26*, 1584−1589.
(33) Wehrenfennig, C.; Liu, M. Z.; Snaith, H. J.; Johnston, M. B.; Herz, L. M. Homogeneous Emission Line Broadening in the Organo Lead Halide Perovskite CH3NH3PbI3-xClx. *J. Phys. Chem. Lett.* **2014**, *5*, 1300−1306.
(34) Milot, R. L.; Eperon, G. E.; Snaith, H. J.; Johnston, M. B.; Herz, L. M. Temperature-Dependent Charge-Carrier Dynamics in $CH_3NH_3PbI_3$ Perovskite Thin Films. *Adv. Funct. Mater.* **2015**, *25*, 6218−6227.
(35) Wright, A. D.; Verdi, C.; Milot, R. L.; Eperon, G. E.; Perez-Osorio, M. A.; Snaith, H. J.; Giustino, F.; Johnston, M. B.; Herz, L. M. Electron-Phonon Coupling in Hybrid Lead Halide Perovskites. *Nat. Commun.* **2016**, *7*, 11755.
(36) Lloyd-Hughes, J.; Jeon, T. I. A Review of the Terahertz Conductivity of Bulk and Nano-Materials. *J. Infrared, Millimeter, Terahertz Waves* **2012**, *33*, 871−925.
(37) Ulbricht, R.; Hendry, E.; Shan, J.; Heinz, T. F.; Bonn, M. Carrier Dynamics in Semiconductors Studied with Time-Resolved Terahertz Spectroscopy. *Rev. Mod. Phys.* **2011**, *83*, 543−586.
(38) Beard, M. C.; Turner, G. M.; Schmuttenmaer, C. A. Transient Photoconductivity in GaAs as Measured by Time-Resolved Terahertz Spectroscopy. *Phys. Rev. B: Condens. Matter Mater. Phys.* **2000**, *62*, 15764−15777.
(39) Pidgeon, C. R.; Ciesla, C. M.; Murdin, B. N. Suppression of Non-radiative Processes in Semiconductor Mid-infrared Emitters and Detectors. *Prog. Quantum Electron.* **1997**, *21*, 361−419.
(40) Shockley, W.; Read, W. T. Statistics of the Recombinations of Holes and Electrons. *Phys. Rev.* **1952**, *87*, 835−842.
(41) Wetzelaer, G.; Scheepers, M.; Sempere, A. M.; Momblona, C.; Avila, J.; Bolink, H. J. Trap-Assisted Non-Radiative Recombination in Organic-Inorganic Perovskite Solar Cells. *Adv. Mater.* **2015**, *27*, 1837−1841.
(42) Saba, M.; Cadelano, M.; Marongiu, D.; Chen, F. P.; Sarritzu, V.; Sestu, N.; Figus, C.; Aresti, M.; Piras, R.; Lehmann, A. G.; et al. Correlated Electron-Hole Plasma in Organometal Perovskites. *Nat. Commun.* **2014**, *5*, 5049.
(43) Sheik-Bahae, M.; Epstein, R. I. Can Laser Light Cool Semiconductors? *Phys. Rev. Lett.* **2004**, *92*, 247403.
(44) Even, J.; Pedesseau, L.; Jancu, J. M.; Katan, C. DFT and k. p Modelling of the Phase Transitions of Lead and Tin Halide Perovskites for Photovoltaic Cells. *Phys. Status Solidi RRL* **2014**, *8*, 31−35.
(45) Umari, P.; Mosconi, E.; De Angelis, F. Relativistic GW Calculations on $CH_3NH_3PbI_3$ and $CH_3NH_3SnI_3$ Perovskites for Solar Cell Applications. *Sci. Rep.* **2014**, *4*, 4467.
(46) Even, J.; Pedesseau, L.; Jancu, J. M.; Katan, C. Importance of Spin-Orbit Coupling in Hybrid Organic/Inorganic Perovskites for Photovoltaic Applications. *J. Phys. Chem. Lett.* **2013**, *4*, 2999−3005.
(47) Haug, A. Temperature Dependence of Auger Recombination in Gallium Antimonide. *J. Phys. C: Solid State Phys.* **1984**, *17*, 6191−6197.
(48) Lingk, C.; von Plessen, G.; Feldmann, J.; Stock, K.; Arzberger, M.; Bohm, G.; Amann, M. C.; Abstreiter, G. Dynamics of Amplified Spontaneous Emission in InAs/GaAs Quantum Dots. *Appl. Phys. Lett.* **2000**, *76*, 3507−3509.
(49) Takahashi, Y.; Hasegawa, H.; Takahashi, Y.; Inabe, T. Hall Mobility in Tin Iodide Perovskite $CH_3NH_3SnI_3$: Evidence for a Doped Semiconductor. *J. Solid State Chem.* **2013**, *205*, 39−43.
(50) Hutter, E. M.; Eperon, G. E.; Stranks, S. D.; Savenije, T. J. Charge Carriers in Planar and Meso-Structured Organic-Inorganic Perovskites: Mobilities, Lifetimes, and Concentrations of Trap States. *J. Phys. Chem. Lett.* **2015**, *6*, 3082−3090.
(51) Shao, Y. H.; Xiao, Z. G.; Bi, C.; Yuan, Y. B.; Huang, J. S. Origin and Elimination of Photocurrent Hysteresis by Fullerene Passivation in $CH_3NH_3PbI_3$ Planar Heterojunction Solar Cells. *Nat. Commun.* **2014**, *5*, 5784.
(52) Stoumpos, C. C.; Malliakas, C. D.; Kanatzidis, M. G. Semiconducting Tin and Lead Iodide Perovskites with Organic Cations: Phase Transitions, High Mobilities, and Near-Infrared Photoluminescent Properties. *Inorg. Chem.* **2013**, *52*, 9019−9038.
(53) deQuilettes, D. W.; Koch, S.; Burke, S.; Paranji, R. K.; Shropshire, A. J.; Ziffer, M. E.; Ginger, D. S. Photoluminescence Lifetimes Exceeding 8 μs and Quantum Yields Exceeding 30% in Hybrid Perovskite Thin Films by Ligand Passivation. *ACS Energy Letters* **2016**, *1*, 438−444.
(54) Sze, S. M.; Lee, M. K. *Semiconductor Devices: Physics and Technology*, 3rd ed.; John Wiley & Sons: Hoboken, NJ, 2012.

DOI: 10.1021/acs.jpclett.6b02030
J. Phys. Chem. Lett. 2016, 7, 4178−4184